Desalination and Water Treatment
www.deswater.com

7 (2009) 93–110

1944-3994 / 1944-3986

Improved approach to steady state simulation of multi-effect distillation plants

Andreas Trostmann

ILF Consulting Engineers, Erdberg Str. 52-60, 1030 Vienna, Austria
Tel. +43 1 713 92 32-467; Fax +43 1 713 92 32-499; email: andreas.trostmann@ilf.com

Received 29 September 2008; Accepted in revised form 14 April 2009

ABSTRACT

Over the past years the landscape of process simulation has tremendously changed. Based on increasingly powerful hardware and improved software applications simulation has come to a new dimension. In order to stay abreast of these changes the OPUS™ simulation program has been developed. Against the top-down philosophy of earlier simulation programs this tool is based on a bottom-up approach enabling the user to simulate any imaginable process configuration. This paper presents the physical and thermodynamic background the current model library for multi-effect distillation (MED) processes is based on. As the most essential models for computer aided steady-state simulation of MED processes the single MED effect, the final condenser and the thermal vapour compressor are described in detail. Along with governing heat and mass balances implemented heat transfer coefficient correlations for condensation inside horizontal plain tubes as well as falling film evaporation on horizontal plain tubes are discussed and compared. Results show significant differences in heat transfer prediction and the necessity to pay utmost attention to the proper selection of such correlations becomes evident. For thermal vapour compression (TVC) both a theoretically based approach and suppliers' design characteristics were incorporated into the simulation program. From checking the obtained data against each other the theoretical approach arose to be much too conservative, resulting in efficiencies exceeding 100% related to suppliers' design characteristics. Used correlations for physical properties of water, water vapour and seawater are stated and a possible new approach for describing physical properties of seawater based on the fundamental equation for the Gibbs energy is presented. The reliability of the current simulation results is evaluated against several project data provided by diverse EPC contractors. The comparisons show a good agreement and the results are within accuracy that allows reasonable prediction of varying operational conditions. Eventually, an outlook on further simulation enhancements is given.

Keywords: Process simulation; Thermal desalination; Multi-effect distillation (MED); Heat transfer; Thermal vapour compression; OPUS™

1. Introduction

Over the past years the landscape of process simulation has tremendously changed. Based on increasingly powerful hardware and improved software applications simulation has come to a new dimension.

In order to stay abreast of these changes the OPUS™ simulation program has been developed, a comprehensive and powerful simulation tool that combines thermodynamic simulation, CAPEX and OPEX estimation, financial modelling, plant optimization and life-cycle cost assessment for combined desalination and power plants [1].

Presented at EuroMed 2008, Desalination for Clean Water and Energy Cooperation among Mediterranean Countries of Europe and the MENA Region, 9–13 November 2008, King Hussein Bin Talal Convention Center, Dead Sea, Jordan.

Against the top-down philosophy of earlier simulation programs this tool is based on a bottom-up approach, meaning that the simulation is not restricted to a certain range of process configurations but can be built up from single components so that any imaginable process configuration is getting feasible.

The said bottom-up approach gives advantage of much more flexibility over the top-down structure. It enables the user to define his own set of input data and to run the simulation in accordance with his particular project related needs [2].

2. OPUS™ — the simulation program

OPUS™ is based on the commercially available IPSEpro software suite which encompasses among others the so called process simulation environment (PSE) and the model development kit (MDK).

PSE is used to map the entire process by arranging single process components, also referred to as models, managed in a single model library. Each model represents the mathematical description of the thermodynamic processes taking place therein. MDK is the necessary tool that is needed to adapt existing or to define new models. Fig. 1 shows a sample screen shot of the process simulation environment.

Besides a standard steady state solver IPSEpro provides an optimizer, called PSOptimize, which allows the user to carry out formal optimizations in order to find the optimum process parameters for the criteria defined.

2.1. OPUS™

Process simulations are accomplished for optimizing the overall process efficiency. However, the crucial factor the final decision usually rests upon is the economic efficiency.

OPUS™ combines the detailed thermodynamic design with the economic efficiency calculation of a power plant, a desalination plant or even a combined desalination and power plant. Fig. 2 shows the principal architecture of OPUS™.

For economic efficiency calculations use is made of the PSEconomy module. This module utilizes project data calculated in the physical model, e.g. the heat transfer surface and the tube material of a heat exchanger, in order to determine the capital expenditures (CAPEX) of the process equipment and it uses process data as for

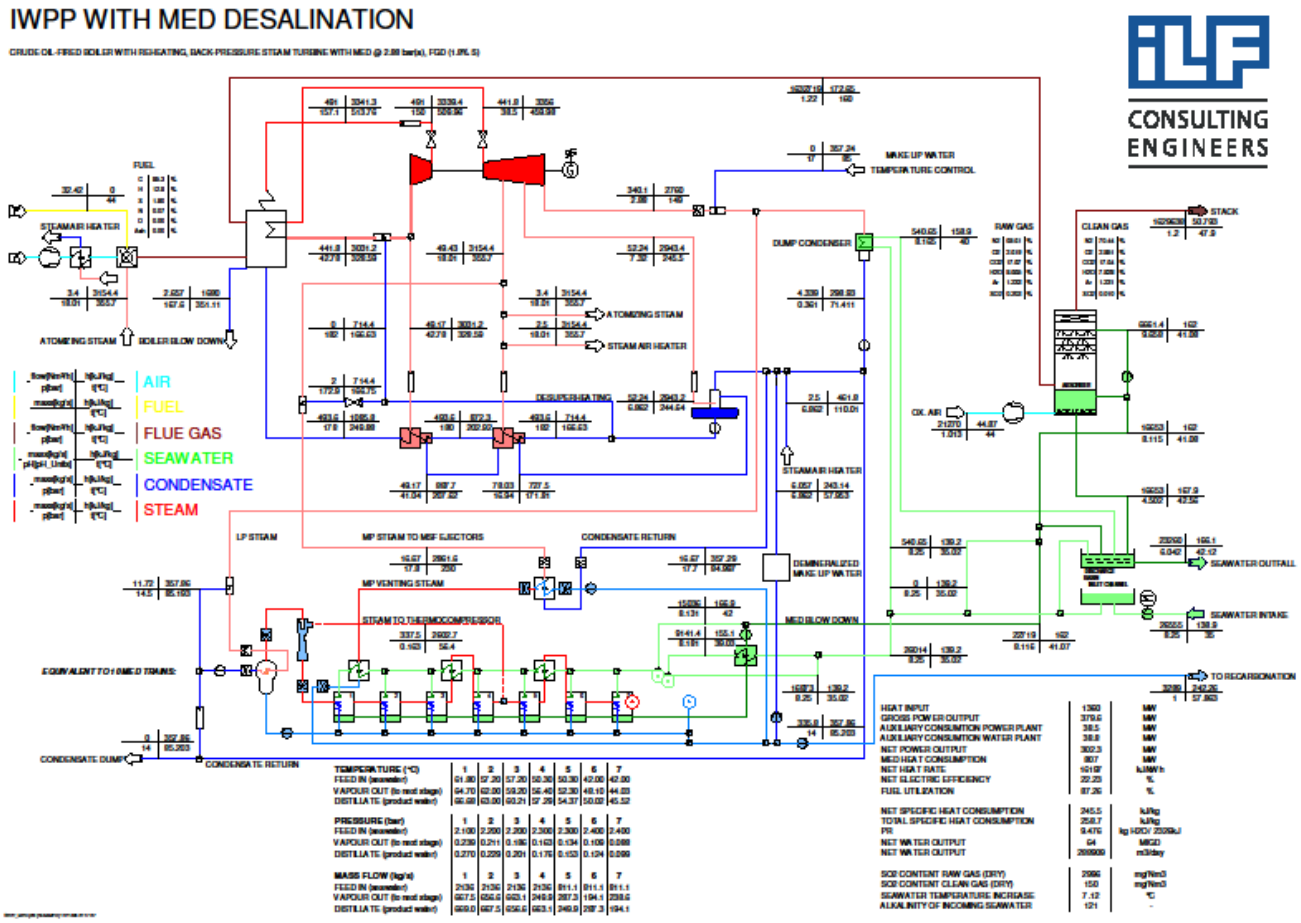

Fig. 1. IPSEpro PSE screen shot.

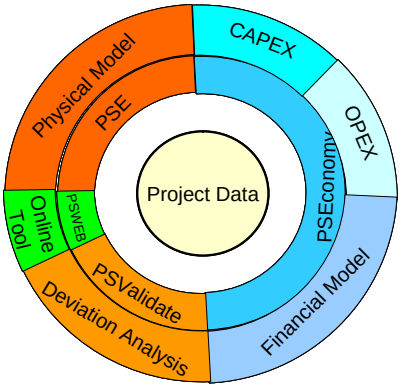

Fig. 2. OPUS™ architecture.

instance the fuel demand in order to get the operational expenditures (OPEX). In the financial model aspects like different operating scenarios, changes in ambient conditions, inflation or taxes are included.

OPUS™ allows the user to optimize and evaluate different process arrangements, different desalination technologies (e.g. MED vs. MSF or RO) and even different financing models based on given operating scenarios and operating parameters.

3. Modelling basics

3.1. Physical properties

Seawater is made up of a wide variety of components. Whereas the total amount of salts dissolved may vary within in a wide range depending on local and seasonal conditions, the chemical composition differs almost negligibly [3].

Although each single component influences the physical properties of seawater to a different extend, most approaches for the calculation of seawater properties are falling back on the idea that the chemical composition of seawater from different parts of the world is very similar. To simplify matter they are represented as a function of salinity, temperature and pressure [4]. Although this principle first introduced by Marcet in 1820 is a good approximation, it is important not to lose sight of the limits of this approximation.

These approaches are generally of empirical nature, mainly using standard seawater as their base. However, attention has to be paid to the different definitions for standard seawater and the different salinity scales existing in the literature, causing sometime different and inconsistent approaches for the theoretical description of seawater properties.

The commercially available desalination library of IPSEpro includes approaches from Grunberg (1970) for the density, the specific enthalpy and the boiling point elevation of seawater [5]. These approaches were adapted in such a manner that they merge with pure water properties for infinite solutions. Properties for pure water were taken from IAPWS 1997 standards [6].

In order to enable a more comprehensive calculation of the processes taking place during multi effect distillation, OPUS™ was enhanced by implementing approaches from Wangnick for the dynamic viscosity of saturated steam [7], from Hoemig for the dynamic viscosity of pure water and seawater [8], from OSW Report No 363 (1968) for thermal conductivity of pure water and seawater [5] and from Grundberg (1970) for the specific heat capacity of pure water and seawater [5].

3.2. Heat transfer coefficients

The overall heat transfer coefficient related to the outer tube surface reads as follows:

$$\frac{1}{U_{\text{overall}}} = \frac{d_o}{d_i}\frac{1}{\alpha_{i,\text{red}}} + \text{FF} + \frac{d_o \ln\left(\frac{d_o}{d_i}\right)}{2\lambda_W} + \frac{1}{\alpha_o} \quad (1)$$

Possible fouling is represented by the corresponding fouling factor (FF). Allowance for present non-condensable gases and their negative influence on heat transfer is made with $\alpha_{i,\text{red}} = \alpha_i \cdot C_{\text{NC-Gas}}$.

3.2.1. Condensation inside horizontal plain tubes

The heat transfer coefficient is strongly dependent on local vapour quality and flow velocities. A two-phase flow regime is encountered depending on the quantities and the physical properties of the fluids flowing as well as the geometric configuration and the kind of heat transfer involved.

At high vapour flow velocities the condensate forms a liquid film on the perimeter of the tube. The prevailing flow regime is called “annular”. With proceeding condensation the vapour flow velocity decreases enabling the condensate draining downwards the tube wall, forming a thicker layer at the bottom than on the top. The increasing condensate mass flow leads to “slug” flow until the entire vapour is converted. In case the condensate does not fully cover the cross-section vapour may pass the tube without condensing (see Fig. 3).

Recommended by the VDI Waermeatlas [10] the flow map by Breber et al. (1980) was chosen in the present work to determine the flow regime predominant in multi-effect distiller tubes. Breber et al. bring the different flow pattern into relationship with the modified Froude number Fr_G^* and the flow parameter F.

$$F = \frac{\max\left\{\left(2 \cdot \text{Re}_{l,x}\right)^{0.5}; 0.132 \cdot \text{Re}_{l,x}^{0.9}\right\}}{\text{Re}_{v-l}^{0.9}} \cdot \frac{\eta_l}{\eta_v}\sqrt{\frac{\rho_v}{\rho_l}} \quad (2)$$

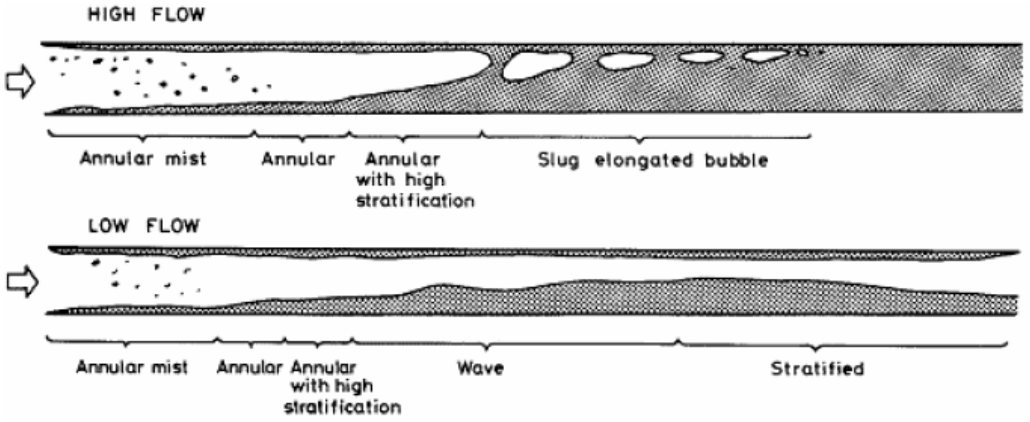

Fig. 3. Flow patterns encountered during condensation inside horizontal tubes [9].

$$\mathrm{Re}_{l,x} = \frac{\dot{\Gamma}_x}{\eta_l} \cdot \frac{\dot{m}_{l,x}}{\pi d \eta_l} \tag{3}$$

$$\mathrm{Re}_{v-l} = \frac{u_{v-l} \cdot d_h}{\nu_v} \tag{4}$$

$$Fr_G^* = \sqrt{\frac{\rho_v}{\rho_l - \rho_v}} \cdot \frac{\overline{u}_{v,0}}{\sqrt{d \cdot g}} \tag{5}$$

The flow chart elaborated enables the distinction between separated flows (annular and stratified) and pure discontinued flow patterns (bubble, slug and plug).

Fig. 4 shows the correlation between the modified Froude number and the flow parameter for conditions typical in MED desalination plants. The curves are calculated for a maximum vapour velocity within the tubes of 50 m/s and for vapour temperatures of 35°C for the last and 80°C for the first effect. The inner tube diameter was assumed to be 19 mm.

The flow pattern during condensation within the tubes turned out to be wavy and stratified for the first effects and to enter the transient flow pattern for the last effects of a multi-effect distillation unit.

Four heat transfer correlations available in the literature and briefly described in the following were investigated in detail and implemented into OPUS™.

3.2.1.1. Boyko and Kruzhilin

Originally developed for condensation inside vertical tubes the approach from Boyko and Kruzhilin [11] might also be applied for horizontal tubes as long as vapour velocities and condensation rates are high enough. Consequently, the applicability of this approach is certainly

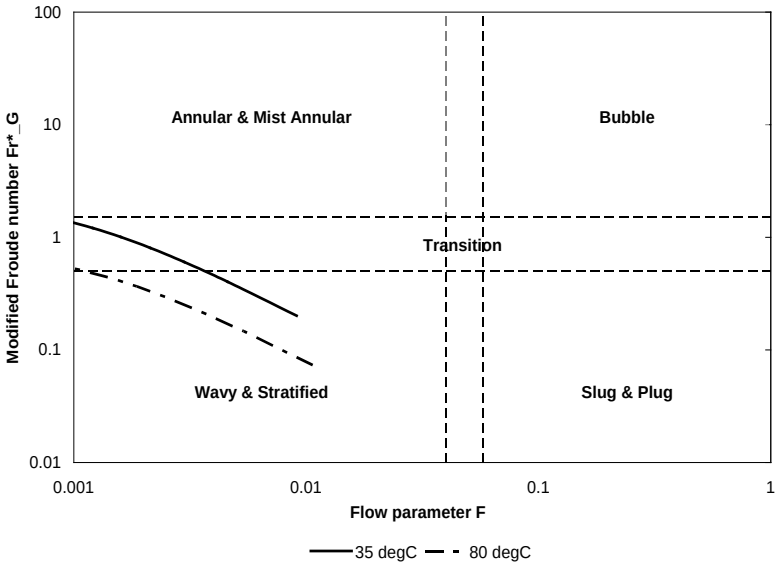

Fig. 4. Predominant flow patter in a MED desalination plant according to Breber et al. [10].

limited, as high mass fluxes cause the internal forces to overcome the gravity forces resulting in an annular flow pattern followed by slug and plug flow which is not the case in MED desalination units according to the Breber et al flow map (see Fig. 4). However, the authors fail to provide appropriate boundaries for the applicability.

$$\alpha_i = \frac{\lambda_l}{d_i} \cdot 0.024 \left(\mathrm{Re}_{l,s}\right)^{0.8} \left(\mathrm{Pr}_l\right)^{0.43} \frac{\sqrt{\left(\frac{\rho}{\rho_m}\right)_{in}} + \sqrt{\left(\frac{\rho}{\rho_m}\right)_{out}}}{2} \tag{6}$$

$$\mathrm{Re}_{l,s} = \frac{\dot{m}}{N_{tubes} \pi \frac{d_i^2}{4}} \frac{d_i}{\eta_l} \tag{7}$$

$$\left(\frac{\rho}{\rho_m}\right)_{in} = 1 + \frac{\rho_l - \rho_v}{\rho_v} x_{in} \tag{8}$$

$$\left(\frac{\rho}{\rho_m}\right)_{out} = 1 + \frac{\rho_l - \rho_v}{\rho_v} x_{out} \tag{9}$$

2.1.2. Jaster and Kosky

The functional correlation introduced by Jaster and Kosky [12] covers stratified flow and is based on the model of Butterworth and Hewitt (1977).

$$\alpha = \frac{\varphi}{\pi} \alpha_\varphi \tag{10}$$

$$\alpha_\varphi = \beta \left(\frac{\lambda_l^3 \rho_l^2 g \left(h_v - h_l\right)}{\eta_l \left(T - T_{wall}\right) d_i} \right)^{0.25} \tag{11}$$

$$\beta = 0.728 \frac{\pi}{\varphi} \left(\frac{\varphi}{\pi} + \frac{\sin\left(2(\pi - \varphi)\right)}{2\pi} \right)^{0.75} \tag{12}$$

Angle φ can be obtained by Eq. (13) with $\varphi = \pi - \Phi$ as per Chadock (1957).

$$\dot{m}_{out} = N_{tubes} \cdot 29.2 \cdot \rho_l M_{H2O} d_i^{3.5} \left(1 - \cos(\Phi)\right)^{3.6} \tag{13}$$

3.2.1.3. Dobson and Chato

Dobson and Chato [9] consider the annular flow pattern in addition to the stratified-wavy flow regime. The equation obtained for the heat transfer coefficient reads as follows:

$$\mathrm{Nu} = \frac{\alpha d_i}{\lambda_l} = \frac{0.23 \mathrm{Re}_v^{0.12}}{1 + 1.11 X_{tt}^{0.58}} \cdot \left[\frac{Ga_l \mathrm{Pr}_l}{Ja_l} \right]^{0.25} + \left(1 - \frac{\varphi}{\pi}\right) \mathrm{Nu}_{strat} \tag{14}$$

$$\mathrm{Nu}_{strat} = 0.0195 \mathrm{Re}_{l,s}^{0.8} \mathrm{Pr}_l^{0.4} \left(1.376 + \frac{C_1}{X_{tt}^{C_2}}\right)^{1/2} \tag{15}$$

$$\mathrm{Re}_v = \frac{4\dot{m}_{total}}{N_{tubes} \pi d_i \eta_v} \tag{16}$$

$$\mathrm{Re}_{l,s} = \frac{4\dot{m}_{total}(1 - x)}{N_{tubes} \pi d_i \eta_l} \tag{17}$$

$$Ga_l = \frac{g \rho_l \left(\rho_l - \rho_v\right) d_i^3}{\eta_l^2} \tag{18}$$

$$Ja_l = \frac{c_{p,l} \left(T_{sat} - T_{wall}\right)}{\Delta h_{evap}} \tag{19}$$

$$X_{tt} = \left(\frac{1 - x}{x}\right)^{0.9} \left(\frac{\rho_v}{\rho_l}\right)^{0.5} \left(\frac{\eta_l}{\eta_v}\right)^{0.1} \tag{20}$$

C_1 and C_2 are empirically found parameters and are read for $0 < F$ 0.7 as follows:

$$C_1 = 4.172 + 5.48 Fr_l - 1.564 Fr_l^2 \tag{21}$$

$$C_2 = 1.773 - 0.169 Fr_l \tag{22}$$

And for $Fr_l > 0.7$

$$C_1 = 7.242 \tag{23}$$

$$C_2 = 1.655 \tag{24}$$

3.2.1.4. VDI Waermeatlas

The approach according to VDI Waermeatlas [10] distinguishes between laminar and turbulent flow and considers both of them.

$$\mathrm{Nu}_{l,x}^* = \sqrt{\left(K_{Ph,lam} \mathrm{Nu}_{l,x,lam}^+\right)^2 + \left(K_{Ph,turb} \mathrm{Nu}_{l,x,turb}^+\right)^2} \tag{25}$$

$$K_{Ph,lam} = 1 + \left(\mathrm{Pr}_l^{0.56} - 1\right) \tanh\left(\tau_v^*\right) \tag{26}$$

$$K_{Ph,turb} = 1 + \left(\mathrm{Pr}_l^{0.08} - 1\right) \tanh\left(\tau_v^*\right) \tag{27}$$

$$\mathrm{Nu}_{l,x,lam}^+ = 0.693 \left(\frac{1 - \frac{\rho_v}{\rho_l}}{\mathrm{Re}_{l,x}} \right)^{\frac{1}{3}} K_w \tag{28}$$

$$\mathrm{Re}_{l,x} = \frac{\dot{m}_{l,x}}{\pi d_i \eta_l} \tag{29}$$

In order to encounter the absence of shear stress caused by gravity the approach for vertical walls is to be modified by K_w that reads as follows:

$$K_w = \sqrt[3]{\tau_v^*} \tag{30}$$

$$\tau_v^* = \frac{\tau_v}{\rho_l g \delta_A^+} \tag{31}$$

$$\tau_v = \frac{\xi_r^0}{8} \rho_v \overline{u}_{v\text{-}l}^2 \tag{32}$$

In Eq. (32) the term u_{v-l} represents the average relative velocity between the vapour and the liquid phase. The resistance coefficient ξ_r obeys to:

$$\xi_{\mathrm{r}}^{0} = \xi_{\mathrm{g}}^{0}(1+850F) \tag{33}$$

$$\xi_{\mathrm{g}}^{0} = 0.184\,\mathrm{Re}_{\mathrm{v\text{-}l}}^{-0.2} \tag{34}$$

$$\mathrm{Re}_{\mathrm{v\text{-}l}} = \frac{\overline{u}_{\mathrm{v\text{-}l}} d_{\mathrm{h}}}{\nu_{\mathrm{v}}} \approx \frac{4\dot{m}_{\mathrm{v,x}}}{\pi d_{\mathrm{i}} \eta_{\mathrm{v}}} \tag{35}$$

$$\varepsilon = \frac{V_{\mathrm{v}}}{V_{\mathrm{v}} + V_{\mathrm{l}}} = 1 - \frac{1}{1 + \dfrac{1}{8.48F}} \tag{36}$$

Valid for $\varepsilon \geq 0.67$ the average fluid thickness can be written as:

$$\delta_{\mathrm{A}}^{+} = \frac{1-\varepsilon}{4} d_{\mathrm{i}} \tag{37}$$

$$\mathrm{Nu}_{\mathrm{l,x,turb}}^{+} = \frac{0.0283 \cdot \mathrm{Re}_{\mathrm{l,x}}^{\frac{7}{24}} \mathrm{Pr}_{\mathrm{l}}^{\frac{1}{3}}}{1 + 9.66 \cdot \mathrm{Re}_{\mathrm{l,x}}^{-\frac{3}{8}} \cdot \mathrm{Pr}_{\mathrm{l}}^{-\frac{1}{6}}} K_{\mathrm{w}} \tag{38}$$

$$\mathrm{Nu}_{\mathrm{l,x}} = \frac{\alpha_{\mathrm{l,x}} L_{\mathrm{Film}}}{\lambda_{\mathrm{l}}} \tag{39}$$

$$L_{\mathrm{Film}} = \sqrt[3]{\frac{\nu_{\mathrm{l}}^{2}}{g}} \tag{40}$$

3.2.1.5. Comparison and discussion

The herein presented heat transfer coefficient approaches show a different development with changing vapour quality (Fig. 5). Whereas Jaster and Kosky [12] predict the heat transfer coefficient to be independent on the vapour quality, the VDI approach yields in a clear decrease with falling vapour content. The approach by Dobson and Chato [9] is at a similar level as the one from Jaster and Kosky [12] but with a slight decrease with diminishing vapour content. Compared to the VDI approach both result in an average heat transfer coefficient some 1.6 times higher. As expected from the flow pattern it is based on, the approach from Boyko and Kruzhilin [11] appears to be inadequate for the predominant conditions.

To simplify matters the heat transfer calculation along the tube is not done incrementally, so an average value for the heat transfer coefficient must to be found as it changes with progressing condensation in dependency of the vapour quality. This average value changes with temperature in case the approach by Dobson and Chato [9] and VDI Waermeatlas [10] is used but remains almost constant for Boyko and Kruzhilin [11] and for Jaster and Kosky [12]. Contrary to the temperature dependency the approaches from Boyko and Kruzhilin [11] and VDI Waermeatlas [10] change with mass flux, whereas the heat transfer coefficients according to Dobson and Chato [9] and Jaster and Kosky [12] remain almost constant.

All these effects were considered and the average heat transfer coefficient for Jaster and Kosky [12] was found to be at a vapour quality of 0.5 kg/kg. For Boyko and Kruzhilin [11] the heat transfer coefficient averaged for condensation temperature and total mass flux is assessed to be at a vapour quality of 0.44 kg/kg, whereas the mean for Dobson and Chato [9] lies at 0.36 kg/kg. The mean heat transfer coefficient according to VDI Waermeatlas is related to a vapour quality of 0.66 kg/kg.

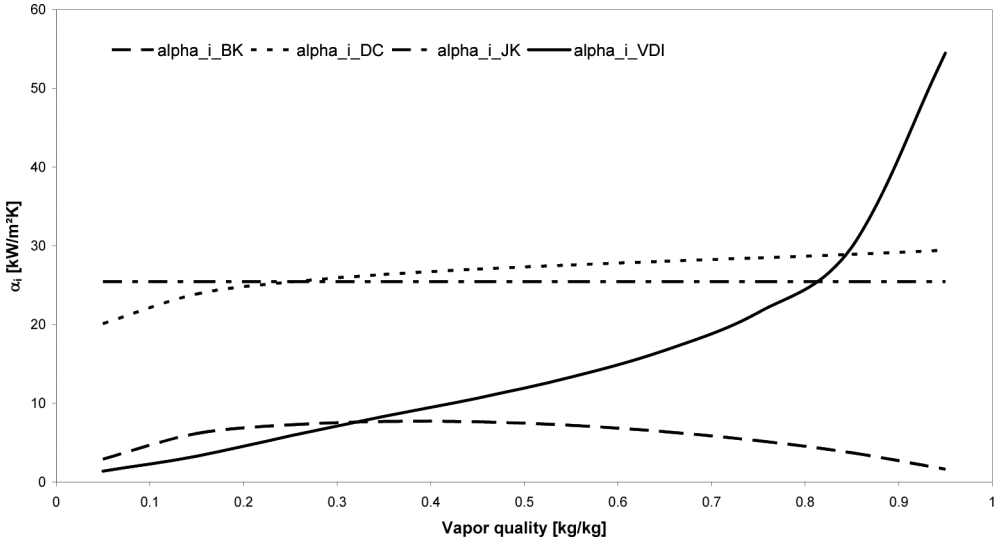

Fig. 5. Comparison of heat transfer coefficients approaches for condensation inside horizontal tubes in dependency of vapour quality (64.0 °C saturation temperature, 15.5 kg/m²s mass flux).

Fig. 6 shows the dependency of the discussed heat transfer models on the mass flux at a saturation temperature of 64°C and a vapour quality of 0.5 kg/kg. The model from VDI, Dobson and Chato as well as from Boyko and Kruzhilin show a very similar development with increasing mass flux. Only Jaster and Kosky predict a decrease.

Also the temperature dependency deviates for the different models (Fig. 7). VDI as well as Boyko and Kruzhilin show a decrease with increasing saturation temperature at constant vapour quality and mass flux, Jaster and Kosky [12] and Dobson and Chato [9] reveal a rising heat transfer coefficient.

Fig. 8 represents the distribution of the vapour quality along a tube. As expected from Fig. 5 the vapour quality for both Dobson and Chato [9] and Jaster and Kosky [12] declines almost linear with the tube length. The average vapour quality is assumed to be in a range of 0.44 kg/kg to 0.45 kg/kg. For the VDI model the average vapour quality is much less as most of the condensation occurs at the tube inlet (Fig. 5) resulting in a low vapour quality in the remaining tube. The average value for the presumed conditions was found to be 0.28 kg/kg. Following the approach from Boyko and Kruzhilin the mean value will be some 0.47 kg/kg.

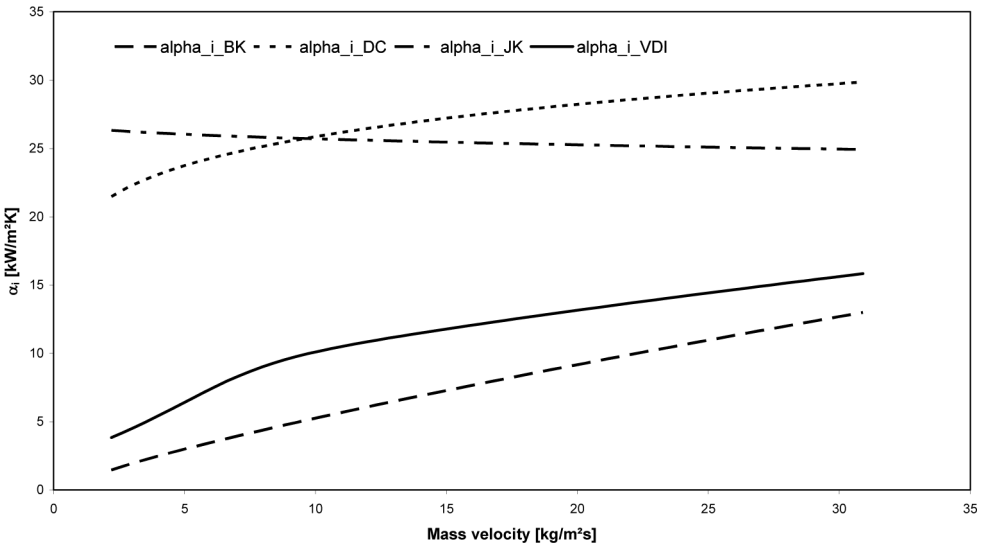

Fig. 6. Comparison of heat transfer coefficient approaches for condensation inside horizontal tubes in dependency of mass flux (64°C saturation temperature, 0.5 kg/kg vapour quality).

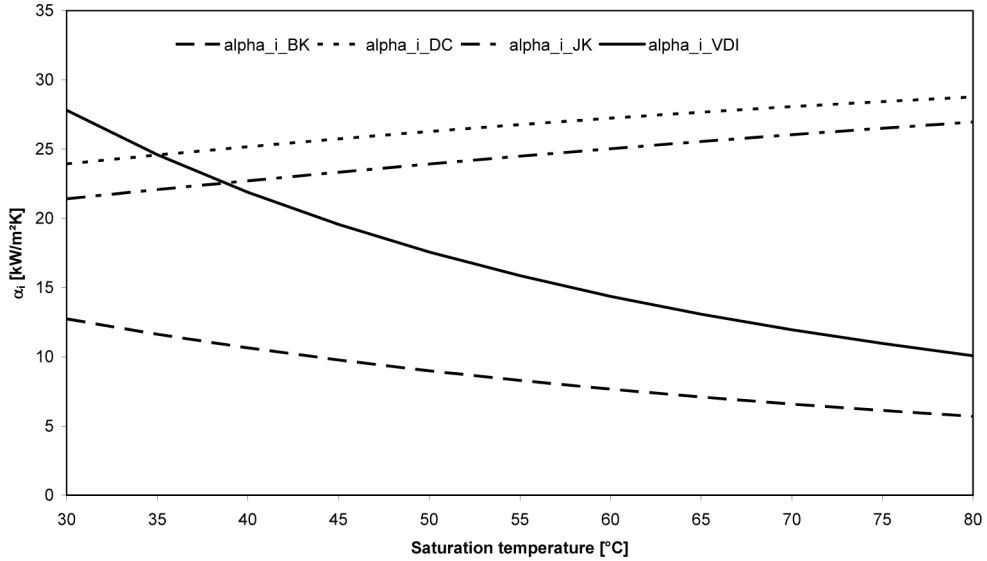

Fig. 7. Comparison of heat transfer coefficient approaches for condensation inside horizontal tubes in dependency of saturation temperature (0.5 kg/kg vapour quality, 15.5 kg/m²s mass flux).

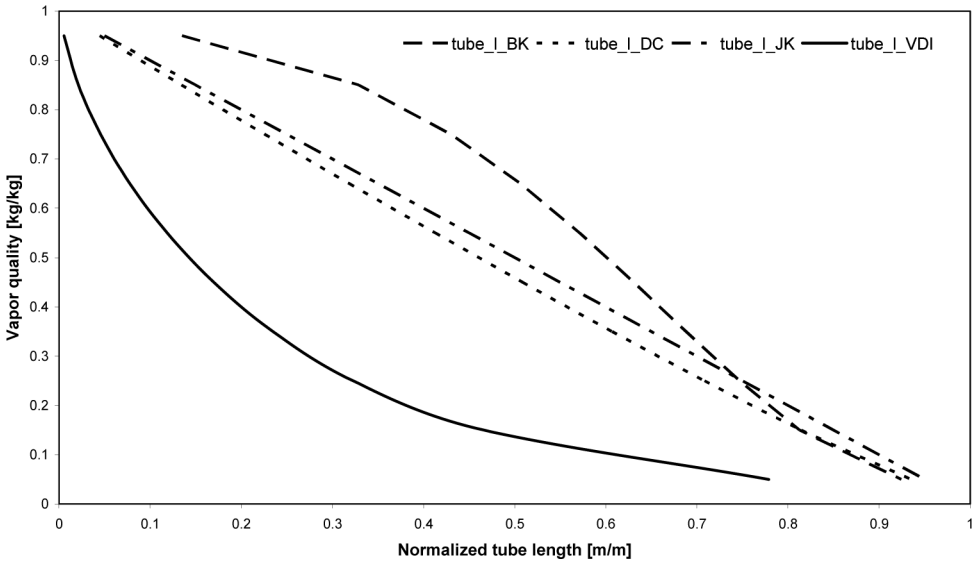

Fig. 8. Distribution of vapour quality along tube length for condensation inside horizontal tubes in dependency of heat transfer coefficient approach (64.0°C saturation temperature, 15.5 kg/m²s mass flux).

3.2.2. Falling film evaporation on horizontal plain tubes

As for the condensation inside a tube knowledge about the flow pattern governing the evaporation of a falling film on horizontal plain tubes is essential.

In general a distinction is drawn between laminar, laminar-wavy and turbulent. Limits for the transition between the different flow modes are differently stated in the literature. However, for application in multi-effect distillers only the laminar and laminar-wavy modes are relevant.

Besides the flow pattern also the heat flux plays a major role. If the heat flux is high enough nucleate boiling occurs, which increases the heat transfer coefficient. On the other hand the formation of dry patches may occur due to bubble formation. This in turn is detrimental to heat transfer. As long as nucleate boiling is avoided the heat transfer is controlled by conduction and convection, irrespective of the flow pattern. Mass flows and corresponding heat fluxes for save operation were investigated by Widua [13].

3.2.2.1. Owens

Correlations from Owens [14] were obtained from experimental investigations on ammonia evaporating on a single plain horizontal tube. For evaporation without nucleate boiling these correlations read as follows:

$$\mathrm{Re_l} < \mathrm{Re_{l,\,turb}} \quad \mathrm{Nu_{lam}} = 2.2\left(\frac{s-d_o}{d_o}\right)^{0.1}\left(2\mathrm{Re_{l,1}}\right)^{-\frac{1}{3}} \tag{41}$$

$$\mathrm{Re_l} > \mathrm{Re_{l,\,turb}} \quad \mathrm{Nu_{turb}} = 0.185\left(\frac{s-d_o}{d_o}\right)^{0.1}\mathrm{Pr_l}^{0.5} \tag{42}$$

$$\mathrm{Re_{l,1}} = \frac{4\Gamma}{\eta_l} \tag{43}$$

The tentatively laminar-turbulent transition point given by Owens [14] is

$$\mathrm{Re_{l,turb}} = \frac{1680}{2}\mathrm{Pr_l}^{-1.5} \tag{44}$$

Whereby Γ is the spray density and can be written as

$$\Gamma = \frac{\dot{m}}{2L} \tag{45}$$

Eqs. (43) and (44) are valid for Reynolds numbers between 750 and 5000, for Prandtl numbers between 1 and 4 and for ratios of $(s–d_o)/d_o$ between 0.125 and 2.125.

3.2.2.2. Arzt

Theoretical investigations accomplished by Arzt [5] for a horizontal tube bundle yielded in following formulas

$$\mathrm{Re_l} < \mathrm{Re_{lam\text{-}wavy}} \quad \mathrm{Nu_{lam}} = 0.819 \cdot \left(\frac{4}{3}\right)^{\frac{1}{3}}\mathrm{Re_{l,1}}^{-\frac{1}{3}} \tag{46}$$

$$\mathrm{Re_l} > \mathrm{Re_{lam\text{-}wavy}} \quad \mathrm{Nu_{lam\text{-}wavy}} = 0.673 \cdot \mathrm{Re}_{l,1}^{-0.22} \tag{47}$$

with the critical Reynolds number for the transition from laminar to laminar-wavy

$$\mathrm{Re_{lam\text{-}wavy}} = 2.43 \cdot \mathrm{Ka}^{-\frac{1}{11}} \tag{48}$$

and the Kapitza number

$$\mathrm{Ka} = \frac{\eta^4 g}{\rho\sigma^3} \tag{49}$$

For the turbulent flow regime Arzt [5] refers to the correlation by Chun and Seban [15]

$$\mathrm{Re_l} > \mathrm{Re_{l,\,turb}} \quad N_{\mathrm{turb}} = 3.8e^{-3}\,\mathrm{Re_{l,1}^{0.4}\,Pr_l^{0.65}} \tag{50}$$

with the critical Reynolds number for turbulent flow by Chun and Seban [15]

$$\mathrm{Re_{l,turb}} = 5800 \cdot \mathrm{Pr}^{-1.06} \tag{51}$$

3.2.2.3. Han and Fletcher

Experiments by Han and Fletcher [16] were carried out for medium temperatures of 49–127°C (this equates to Prandtl numbers from 1.3 to 3.6), heat fluxes between 30 and 80 kW/m² and spray densities in the range of 1.16–3.79 cm²/s (this equates to Reynolds numbers from 770 to 7000). The medium investigated was water.

$$Nu = 0.025 \cdot \mathrm{Re_{l,1}^{0.2}\,Pr_l^{0.53}} \tag{52}$$

3.2.2.4. Fujita and Tsutsui

Fujita and Tsutsui [17] investigated the heat transfer during evaporation on an array of five tubes arranged one below the other. The medium was Freon R11 (CCl_3F) with mass fluxes resulting in Reynolds numbers between 10 and 2000. The range of heat fluxes was between 5 and 15 kW/m².

Their approach distinguishes between the heat transfers on the first row, which is lower due to a not fully developed liquid film, and the remaining tube rows.

$$Nu_1 = \sqrt{\mathrm{Re_{l,1}^{-\frac{2}{3}}} + 0.008 \cdot \mathrm{Re_{l,1}^{0.3}\,Pr^{0.25}}} \tag{53}$$

$$Nu_{2-5} = \sqrt{\mathrm{Re_{l,1}^{-\frac{2}{3}}} + 0.01 \cdot \mathrm{Re_{l,1}^{0.3}\,Pr^{0.25}}} \tag{54}$$

For the entire tube bundle the distribution between $\mathrm{Nu_1}$ and $\mathrm{Nu_{2-5}}$ is conservatively assumed to be 1/5 in the comparison made herein after.

$$Nu = 0.2 \cdot Nu_1 + 0.8 \cdot Nu_{2-5} \tag{55}$$

3.2.2.5. Lorenz and Yung

Another approach was developed by Lorenz and Yung [18] differing between a thermal developing region and a fully developed region along the tube perimeter. The average heat transfer coefficient their investigations yielded in is

$$\alpha = \alpha_{\mathrm{th,dev}} \frac{2L_{\mathrm{th}}}{\pi d_{\mathrm{o}}} + \alpha_{\mathrm{th,fully}} \left(1 - \frac{2L_{\mathrm{th}}}{\pi d_{\mathrm{o}}}\right) \tag{56}$$

with $\alpha_{\mathrm{th,dev}}$ representing the thermal developing region, expressed as follows

$$\alpha_{\mathrm{th,dev}} = \frac{3}{8} \frac{c_{\mathrm{p,l}} \Gamma}{L_{\mathrm{th}}} \tag{57}$$

and $\alpha_{\mathrm{th,fully}}$ for the fully developed region, where they make use of the correlations by Chun and Seban [15] for laminar and turbulent flow.

$$\mathrm{Re_l} < \mathrm{Re_{l,\,turb}} \quad N_{\mathrm{lam}} = 0.821 \cdot \mathrm{Re_{l,1}^{-0.22}} \tag{58}$$

$$\mathrm{Re_l} > \mathrm{Re_{l,\,turb}} \quad N_{\mathrm{turb}} = 3.8e^{-3}\,\mathrm{Re_{l,1}^{0.4}\,Pr_l^{0.65}} \tag{59}$$

$$\mathrm{Re_{l,turb}} = 5800 \cdot \mathrm{Pr}^{-1.06} \tag{60}$$

The thermal developing length is assumed by the authors to be

$$L_{\mathrm{th}} = 0.25 \frac{\Gamma c_{\mathrm{p,l}}}{\pi \lambda_{\mathrm{l}}} \left(\frac{3\Gamma \eta_{\mathrm{l}}}{g \rho_{\mathrm{l}}^2} \right)^{\frac{1}{3}} \tag{61}$$

3.2.2.6. Comparison and discussion

Fig. 9 shows the development of the heat transfer approaches for evaporation on horizontal plain tubes dependent on the film Reynolds number.

The figure reveals very impressively the considerable discrepancies between the different models. Whereas Fujita and Tsutsui [17] and Lorenz and Yung [18] predict a very similar heat transfer, the correlation by Arzt [5] yields in much lower numbers. However, experimental investigations by the same author could not confirm the numbers theoretically achieved. The measured heat transfer coefficient was found to be some twenty percent higher.

The behaviour of the different heat transfer models with changing Prandtl number is shown in Fig. 10. Unlike all the others the model by Han and Fletcher [16] is almost independent of the Prandtl number. In general the heat transfer coefficients are predicted to diminish with increasing Prandtl and increasing evaporation temperature in turn.

All presented heat transfer models are independent of the ratio tube pitch to tube diameter expect the one by Owens [14]. This model shows a slight increase with an increasing ratio.

3.3. Thermal vapour compression (TVC)

Additional performance improvement is frequently achieved by thermal vapour compression (TVC). It allows less consumption of steam and/or a lower number of effects required, saving capital expenditures in turn.

A schematic drawing of a TVC, also referred to as steam jet ejector, is shown in Fig. 11. The figure represents the characteristics of pressure and velocity along such a TVC. Based on the assumption of saturated conditions for the suction fluid changes in state occurring in a vapour compressor can be seen.

Motive steam (A) coming from an external source with pressure p_1 is expanded in a Laval type nozzle. By expanding part of pressure energy is converted to kinetic energy

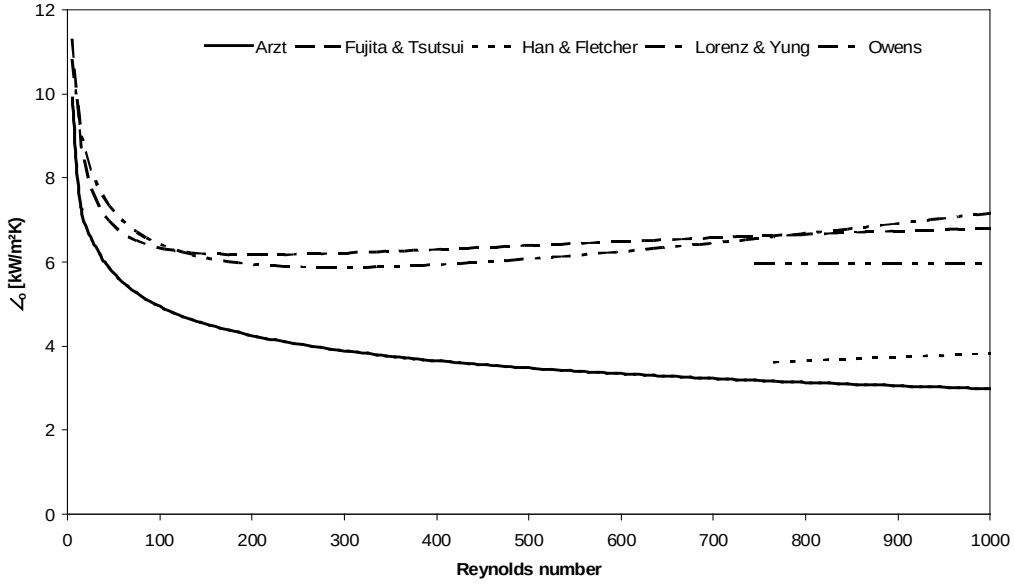

Fig. 9. Comparison of heat transfer coefficient approaches for falling film evaporation on horizontal tubes in dependency of film Reynolds number (64.0°C saturation temperature, 50.0 kW/m² heat flux, 1.25 ratio tube pitch to outer tube diameter).

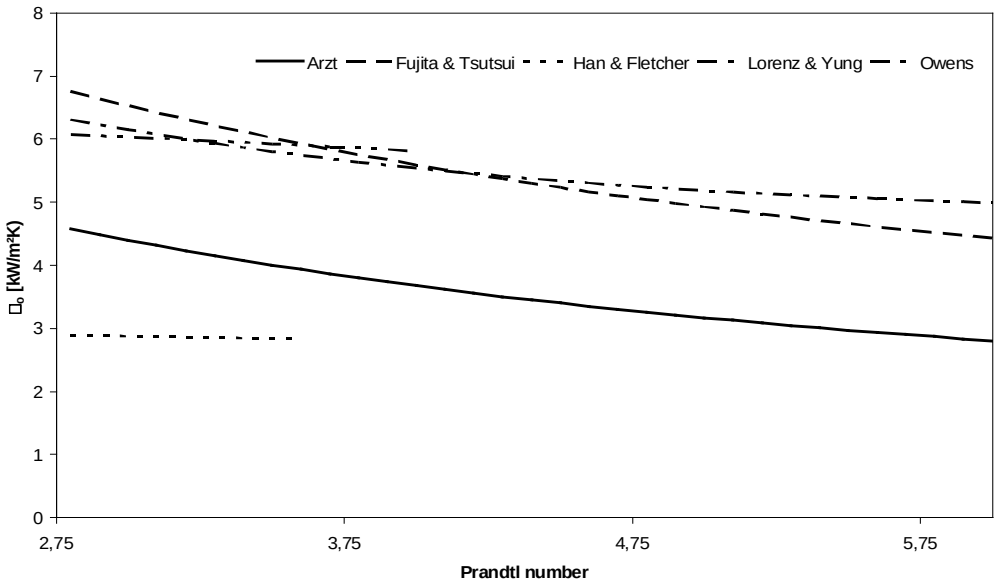

Fig. 10. Comparison of heat transfer coefficient approaches for falling film evaporation on horizontal tubes in dependency of the Prandtl number (0.023 kg/ms mass flow rate of liquid per unit length tube, 50.0 kW/m² heat flux, 1.25 ratio tube pitch to outer tube diameter).

by decreasing pressure (C). The motive steam reaches sound velocity where the flow cross-section is least (B) and is accelerated to supersonic conditions in case the pressure at state (C) is lower than the critical pressure.

The high velocity and the therewith related low pressure cause the suction fluid (D) to be entrained. Both streams are subsequently mixed. The resulting stream (E) is decelerated in a diffuser until it reaches state G, reconverting kinetic energy into pressure.

State E′ represents conditions that would theoretically be reached in case of isentropic expansion both of suction stream (D) and motive steam (A) to state C′. The difference between isentropic and non-isentropic expansion is defined in form of efficiencies.

The correlations integrated in the IPSEpro basic version consider two of such efficiencies, namely the efficiency of the nozzle and the efficiency of the diffuser. This approach is in accordance to Baehr [20] who presumes the

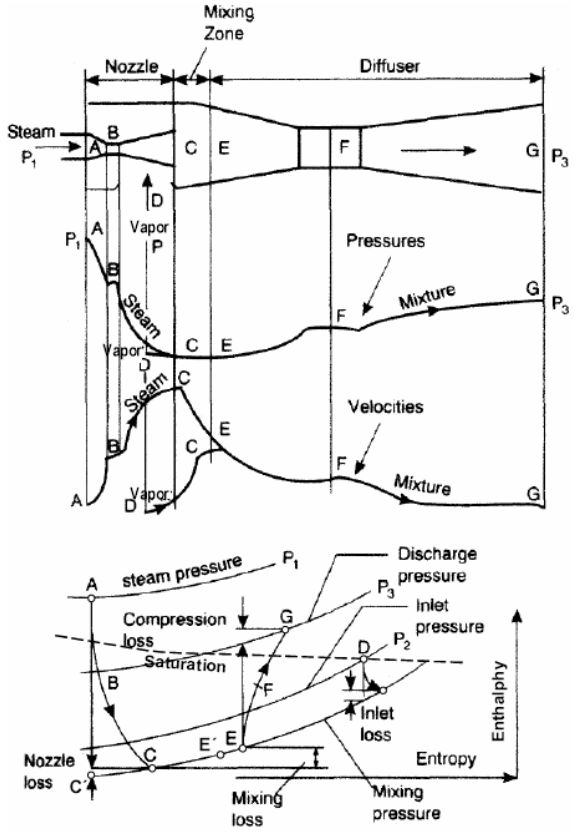

Fig. 11. Schematic drawing of a thermal vapour compressor with typical pressure and velocity characteristics and changes in state during thermal vapour compression (Mollier diagram) [19].

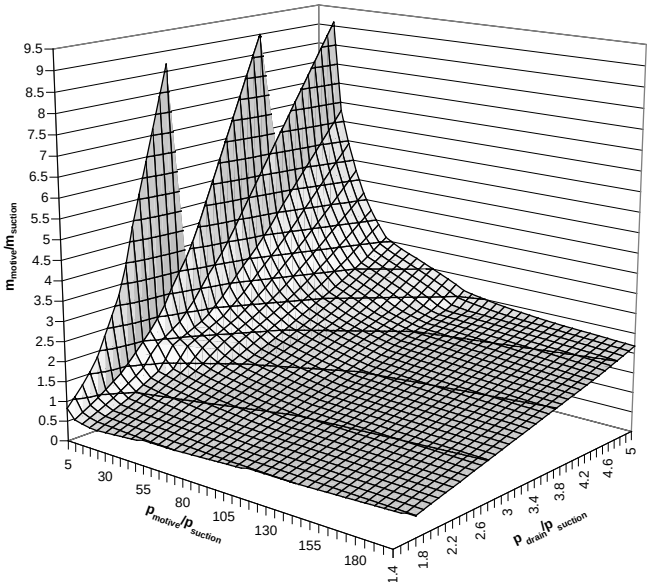

Fig. 12. Mass ratio motive steam to suction steam of a TVC or based on design data by manufacturer A in dependency of the compression ratio and expansion ratio.

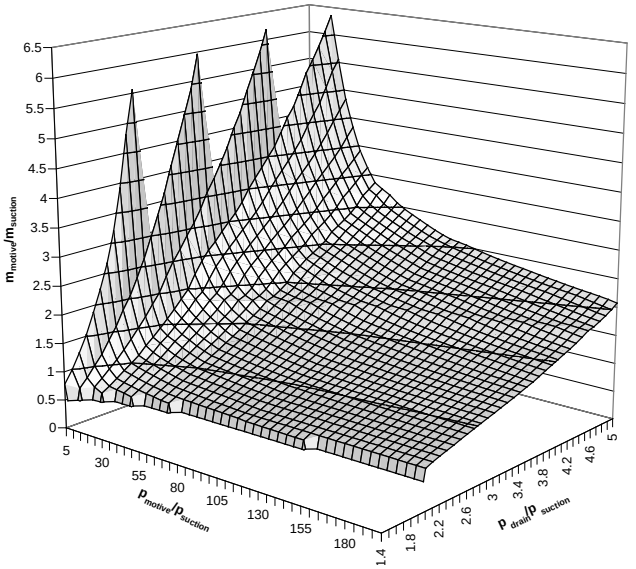

Fig. 13. Mass ratio motive steam to suction steam of a TVC based on design data by manufacturer B in dependency of the compression ratio and expansion ratio.

suction side to be free of losses and the suction pressure to be equal to that of the mixture, which in general is expected to be not the case. Therefore, losses at the suction side are evident and are to be considered as well, resulting in an additional efficiency. Furthermore, Baehr [20] assumes the velocities at the suction side and the outlet to be negligible. However, velocities of up to 80 m/s might be reached in the suction sided cross sectional area for instance, so that this simplification means neglecting a considerable part of the energy brought to the process.

Calculating the overall efficiency based on the approach by Baehr [20] and data from different manufacturers shows that under certain circumstances this efficiency can also exceed 100%. Thus, this approach was abandoned for further proceedings in the present work.

Instead, design characteristics from different manufacturers were implemented and used for calculations. Figs. 12 and 13 exemplify the mass ratio of motive to suction steam flow in dependency of the compression ratio ($p_{drain}/p_{suction}$) and expansion ratio ($p_{motive}/p_{suction}$) of manufacturer A and B.

Figs. 14 and 15 indicate the development of the total efficiency of a thermal vapour compressor in dependency of the compression ratio ($p_{drain}/p_{suction}$) and expansion ratio ($p_{motive}/p_{suction}$). The unevenness comes from reading inaccuracies.

4. Modelling the multi-effect distillation process

A typical multi-effect distillation process inclusive thermal vapour compression (MED-TVC) is schematically

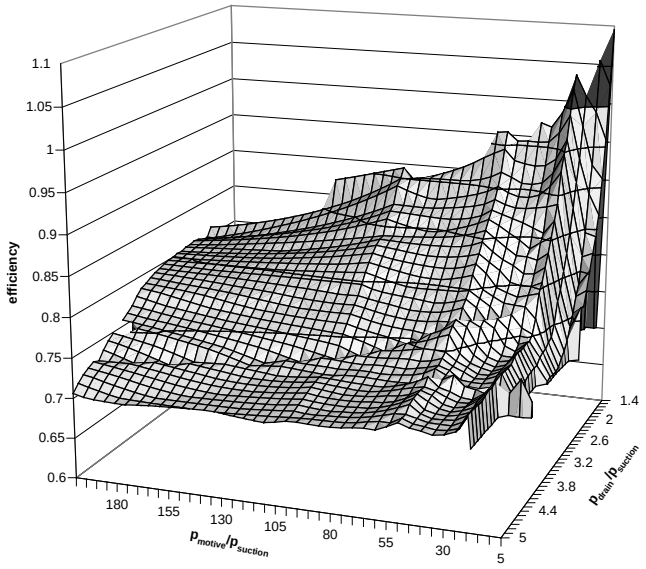

Fig. 14. Total efficiency of a TVC based on the approach by Baehr [20] and supplier A in dependency of the compression ratio and expansion ratio.

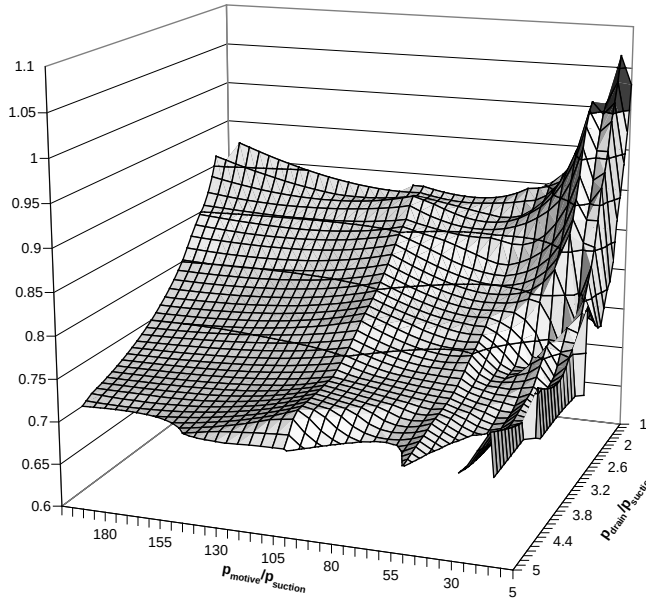

Fig. 15. Total efficiency of a TVC based on the approach by Baehr [20] and supplier B in dependency of the compression ratio and expansion ratio.

shown in Fig. 16. It generally comprises the evaporator consisting of several effects, the final condenser, the thermal vapour compressor and the different process-related pumps.

In the case of simple MED process the thermal vapour compression is omitted and the motive steam is directly fed to the first effect for being used as heating steam.

4.1. Single MED-effect

Make-up water (feed_rw) is sprayed over the heat exchanger tube bundles creating a liquid falling film on the outside of the horizontally arranged tubes. Flowing downwards part of the make-up water is evaporated (steam_rw) thus increasing the salt content of the remaining water, now called brine (brine_rw).

This brine collected at the bottom of the effect and mixed with the brine of the previous effect (feed_br) is directed to the next effect (drain_br), where it faces lower pressure causing it to flash off. The thereby released vapour (steam_br) contributes to the total vapour produced in the relevant stage (drain_steam) which is led through mist eliminators in order to separate remaining water droplets.

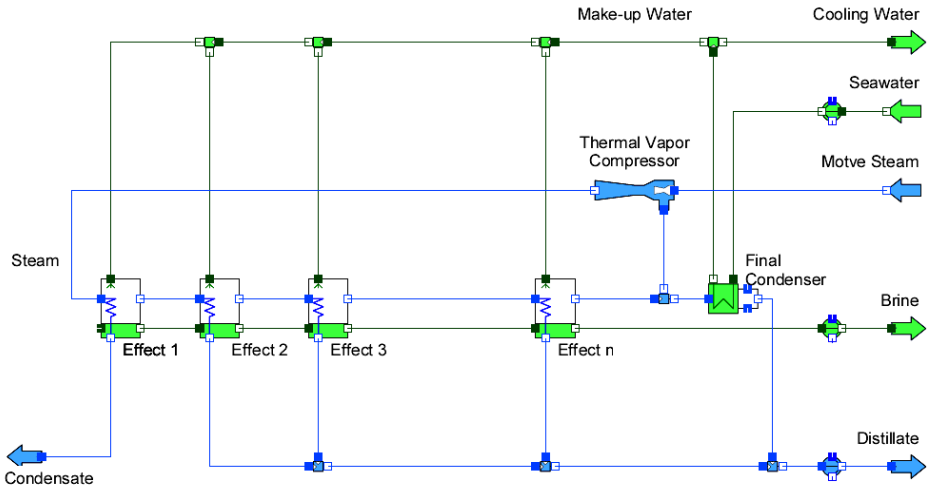

Fig. 16. Typical MED process flow diagram.

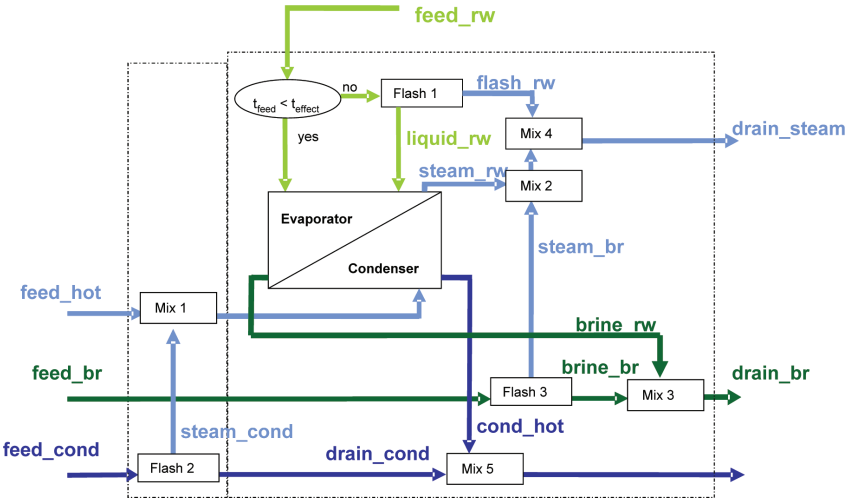

Fig. 17. Schematic flow diagram of a single multi-effect distillation effect.

Once exempt from remaining water droplets, the entire vapour is directed to the tube bundle of the next effect (feed_hot), where it is condensed inside producing a nearly equal mass flow of vapour on the outside of the tubes (steam_rw) from make-up water (feed_rw) being sprayed on the top of the tube bundle.

The vapour condensed (cond_hot) is collected at the bottom of the effect, mixed with distillate coming from the previous effect (drain_cond) and forwarded to the next effect. There it is forced to partially evaporate by lower pressure conditions (steam_cond) forming part of the vapour condensed within in the tubes of the relevant effect.

In case the make-up water is of higher temperature than that related to the saturation pressure prevailing in the effect, part of the make-up water flashes (flash_rw).

Procedures described above were brought into a schematic flow diagram shown as unit operations (Fig. 17).

4.1.1. Make-up water flash (Flash 1)

4.1.1.1. Mass balance

$$\dot{m}_{feed\_rw} = \dot{m}_{liquid\_rw} + \dot{m}_{flash\_rw} \quad (62)$$

$$\dot{m}_{feed\_rw} w_{feed\_rw} = \dot{m}_{liquid\_rw} w_{liquid\_rw} \quad (63)$$

4.1.1.2. Energy balance

$$\dot{m}_{feed\_rw} h_{feed\_rw} = \dot{m}_{liquid\_rw} h_{liquid\_rw} + \dot{m}_{flash\_rw} h_{flash\_rw} \quad (64)$$

The process is assumed to be adiabatic. Losses due to possible condensation on parts of the evaporator like the shell or internals are neglected so that the produced vapour is fully forwarded to the next effect where it acts as heating steam.

Provided that the process has enough time to reach equilibrium both the pressures as well as the temperatures of the flashed vapour and the remaining seawater are equal. In case not, a certain non-equilibrium allowance has to be considered.

In case the temperature of the fed make-up water is below the temperature related to the saturation pressure of the effect, no flash occurs ($\dot{m}_{flash\_rw} = 0$).

4.1.2. Distillate flash (Flash 2)

4.1.2.1. Mass balance

$$\dot{m}_{feed\_cond} = \dot{m}_{drain\_cond} + \dot{m}_{steam\_cond} \quad (65)$$

4.1.2.2. Energy balance

$$\dot{m}_{feed\_cond} h_{feed\_cond} = \dot{m}_{drain\_cond} h_{drain\_cond} + \dot{m}_{steam\_cond} h_{steam\_cond} \quad (66)$$

The process is assumed to be adiabatic. Losses due to possible condensation on parts of the evaporator like the shell or internals are neglected. The vapour gained from the distillate flash contributes to the evaporation process by being condensed inside the tubes of the particular effect. Equilibrium conditions are taken for granted.

4.1.3. Brine flash (Flash 3)

4.1.3.1. Mass balance

$$\dot{m}_{feed\_br} = \dot{m}_{brine\_br} + \dot{m}_{steam\_br} \quad (67)$$

$$\dot{m}_{feed\_br} w_{feed\_br} = \dot{m}_{brine\_br} w_{brine\_br} \quad (68)$$

4.1.3.2. Energy balance

$$\dot{m}_{feed\_br} h_{feed\_br} = \dot{m}_{brine\_br} h_{brine\_br} + \dot{m}_{steam\_br} h_{steam\_br} \quad (69)$$

The process is assumed to be adiabatic. The brine when being brought in contact with the vapour phase of the effect appropriately and for a sufficient period reaches equilibrium conditions. Where this is not given,

a suitable approach considering this non-equilibrium has to be implemented.

Furthermore, it is assumed that the vapour produced does not interact with the brine flowing counter current and that the entire mass flow produced is forwarded to the next effect, acting there as heating steam.

4.1.4. Condenser including heating steam mixer (Mix 1)

4.1.4.1. Mass balance

$$\dot{m}_{\text{feed\_hot}} + \dot{m}_{steam\_cond} = \dot{m}_{\text{cond\_hot}} \tag{70}$$

4.1.4.2. Energy balance

$$\dot{m}_{\text{feed\_hot}} h_{\text{feed\_hot}} + \dot{m}_{\text{steam\_cond}} h_{\text{steam\_cond}} = \dot{m}_{\text{cond\_hot}} h_{\text{cond\_hot}} + Q \tag{71}$$

4.1.5. Brine mixer (Mix 3)

4.1.5.1. Mass balance

$$\dot{m}_{\text{brine\_rw}} + \dot{m}_{\text{brine\_br}} = \dot{m}_{\text{drain\_br}} \tag{72}$$

$$\dot{m}_{\text{brine\_rw}} w_{\text{brine\_rw}} + \dot{m}_{\text{brine\_br}} w_{\text{brine\_br}} = \dot{m}_{\text{drain\_br}} w_{\text{drain\_br}} \tag{73}$$

4.1.5.2. Energy balance

$$\dot{m}_{\text{brine\_rw}} h_{\text{brine\_rw}} + \dot{m}_{\text{brine\_br}} h_{\text{brine\_br}} = \dot{m}_{\text{drain\_br}} h_{\text{drain\_br}} \tag{74}$$

4.1.6. Vapour mixers (Mix 2 and Mix 4)

4.1.6.1. Mass balance

$$\dot{m}_{\text{steam\_rw}} + \dot{m}_{\text{steam\_br}} + \dot{m}_{\text{flash\_rw}} = \dot{m}_{\text{drain\_steam}} \tag{75}$$

4.1.6.2. Energy balance

$$\dot{m}_{\text{steam\_rw}} h_{\text{steam\_rw}} + \dot{m}_{\text{steam\_br}} h_{\text{steam\_br}} + \dot{m}_{\text{flash\_rw}} h_{\text{flash\_rw}} = \dot{m}_{\text{drain\_steam}} h_{\text{drain\_steam}} \tag{76}$$

4.1.7. Condensate mixer (Mix 5)

4.1.7.1. Mass balance

$$\dot{m}_{\text{drain\_hot}} + \dot{m}_{\text{cond\_hot}} = \dot{m}_{\text{drain\_cond}} \tag{77}$$

4.1.7.2. Energy balance

$$\dot{m}_{\text{drain\_hot}} h_{\text{drain\_hot}} + \dot{m}_{\text{cond\_hot}} h_{\text{cond\_hot}} = \dot{m}_{\text{drain\_cond}} h_{\text{drain\_cond}} \tag{78}$$

4.1.8. Evaporator

4.1.8.1. Mass balance

$$\dot{m}_{\text{liquid\_rw}} = \dot{m}_{\text{brine\_rw}} + \dot{m}_{\text{steam\_rw}} \tag{79}$$

4.1.8.2. Energy balance

$$\dot{m}_{\text{liquid\_rw}} h_{\text{liquid\_rw}} + Q = \dot{m}_{\text{brine\_rw}} h_{\text{brine\_rw}} + \dot{m}_{\text{steam\_rw}} h_{\text{steam\_rw}} + Q_{\text{losses}} \tag{80}$$

Q_{losses} represents part of energy dissipated during the processes and is considered as follows:

$$Q_{\text{losses}} = U_{\text{shell}} A_{\text{shell}} \left(t_{\text{effect}} - t_{\text{ambient}} \right) \tag{81}$$

The vapour produced from seawater evaporation is gained at different temperatures, depending on the particular salt content of the brine with which it is in equilibrium, thus resulting in a temperature distribution across the tube bundle. To simplify matters this temperature distribution is assumed to be linear and the produced vapour has a temperature equal to the geometric mean.

4.1.9. Heat transfer area required

Whenever make-up water entering the effect is of lower temperature than the actual effect temperature it runs through a preheating process [Eq. (82)].

$$Q_{\text{pre}} = \dot{m}_{\text{feed\_rw}} \left(h_{\text{brine\_rw}} - h_{\text{liquid\_rw}} \right) \tag{82}$$

This preheating energy has to be provided by condensing vapour in addition to the amount necessary for evaporation. Thus the total energy demand is $Q = Q_{\text{evap}} + Q_{\text{pre}}$. Consequently, part of the heat transfer area is reserved for preheating purposes only.

$$A_{\text{pre}} = \frac{Q_{\text{pre}}}{U_{\text{pre}} \frac{\left(t_{\text{sw\_pre}} - t_{\text{liquid\_rw}} \right)}{\ln\left(\frac{t_{\text{feed\_hot}} - t_{\text{liquid\_rw}}}{t_{\text{cond\_hot}} - t_{\text{sw\_pre}}} \right)}} \tag{83}$$

$$A_{\text{evap}} = \frac{Q_{\text{evap}}}{U_{\text{evap}} \frac{\left(t_{\text{brine\_rw}} - t_{\text{sw\_pre}} \right)}{\ln\left(\frac{t_{\text{feed\_hot}} - t_{\text{sw\_pre}}}{t_{\text{cond\_hot}} - t_{\text{brine\_rw}}} \right)}} \tag{84}$$

Hence the total heat transfer area needed amounts to A_{total} [Eq. (85)], where A_{evap} represents the evaporation portion.

$$A_{\text{total}} = A_{\text{pre}} + A_{\text{evap}} = N_{\text{tubes}} \pi d_{\text{o}} L_{\text{tubes}} \tag{85}$$

It is presumed that the heating steam used for evaporation purposes is available at saturation conditions and is neither wet nor superheated ($x = 1$). Furthermore it is presumed that no subcooling of condensate occurs.

4.2. Final condenser and pre-heater

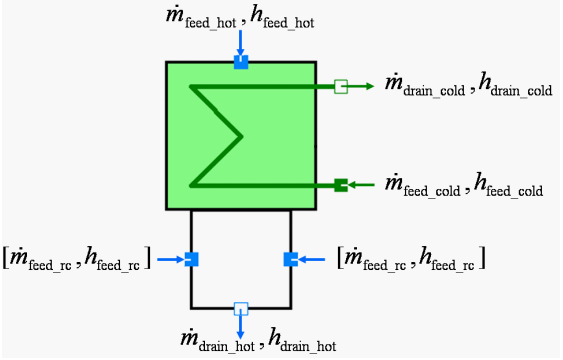

Fig. 18. Condenser representing symbol.

4.2.1. Mass balance

Obeying to the mass conservation the according balances must read:

$$\dot{m}_{\text{feed\_hot}}\left[+\dot{m}_{\text{feed\_rc}}\right]=\dot{m}_{\text{drain\_hot}} \tag{86}$$

Allowance was made for an additional stream that if necessary can be used for dry-run protection of a pump located downstream the condenser ($m_{\text{feed\_rc}}$).

$$\dot{m}_{\text{feed\_cold}}=\dot{m}_{\text{drain\_cold}} \tag{87}$$

$$w_{\text{feed\_cold}}=w_{\text{drain\_cold}} \tag{88}$$

4.2.2. Energy balance

$$\dot{m}_{\text{feed\_hot}}h_{\text{feed\_hot}}\left[+\dot{m}_{\text{feed\_rc}}h_{\text{feed\_rc}}\right]=\dot{m}_{\text{drain\_hot}}h_{\text{drain\_hot}}+Q \tag{89}$$

$$\dot{m}_{\text{feed\_cold}}h_{\text{feed\_cold}}+Q=\dot{m}_{\text{drain\_cold}}h_{\text{drain\_cold}} \tag{90}$$

Q represents the heat transferred, which is also given by following equation:

$$Q=U_{overall}\cdot A_{heat\_trans}\cdot\Delta t_{\log} \tag{91}$$

Usage of inter-stage pre-heaters is widely spread in MED as well as MED-TVC processes for performance improvement. The concept of pre-heaters used is equal to that of the final condenser, precipitating the vapour on the outer tube surface, so that the model discussed herein can be applied for both of them.

4.3. Thermal vapour compressor

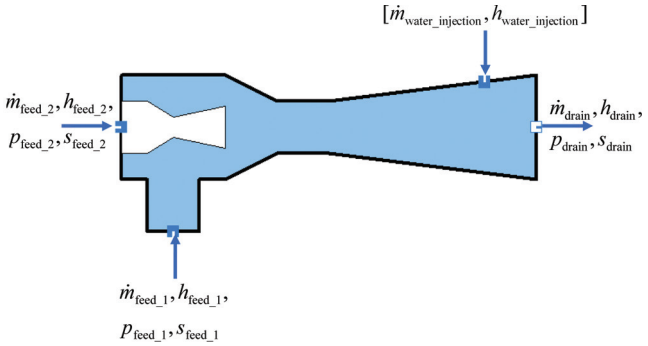

Fig. 19. Symbol representing thermal vapour compressor.

4.3.1. Mass balance

$$\dot{m}_{\text{feed\_1}}+\dot{m}_{\text{feed\_2}}+\dot{m}_{\text{water\_injection}}=\dot{m}_{\text{drain}} \tag{92}$$

4.3.2. Heat balance

$$\dot{m}_{\text{feed\_1}}h_{\text{feed\_1}}+\dot{m}_{\text{feed\_2}}h_{\text{feed\_2}}+\dot{m}_{\text{water\_injection}}h_{\text{water\_injection}}=\dot{m}_{\text{drain}}h_{\text{drain}} \tag{93}$$

Entropy balance

$$\dot{m}_{\text{drain}}s_{\text{drain}}-\left(\dot{m}_{\text{feed\_1}}s_{\text{feed\_1}}+\dot{m}_{\text{feed\_2}}s_{\text{feed\_2}}\right)=\dot{S}_{\text{irreversible}} \tag{94}$$

Following characteristic pressure ratios can be defined:

$$r_{\text{compression}}=\frac{p_{\text{drain}}}{p_{\text{feed\_1}}} \tag{95}$$

$$r_{\text{expansion}}=\frac{p_{\text{feed\_2}}}{p_{\text{feed\_1}}} \tag{96}$$

5. Data evaluation

In order to prove the accuracy and reliability of the developed models several existing desalination plants of varying manufacturers were chosen and the simulation results were compared with manufacturers' data.

Exemplarily, the results for one of these plants are depicted in the following. Fig. 21 shows the simulated mass flows against manufacturer's data for the design case; Fig. 22 shows the same for temperatures. Best results where achieved by slightly adjusting correlations from Jaster and Kosky [12] for the inner and from Fujita and Tsutsui [17] for the outer heat transfer coefficient. Predictions for mass flows and temperatures were in the range of ±2.1% as shown in Figs. 20–23.

For calculating off-design cases tube bundle geometries obtained from the design case were kept and process parameters were changed accordingly. Figs. 22 and 23 include minimum distillate capacity (40%) combined with maximum (34°C) and minimum (28°C) seawater temperature as well as the combination of maximum capacity and minimum temperature. Results were in the range of ±4.3% for all off-design cases.

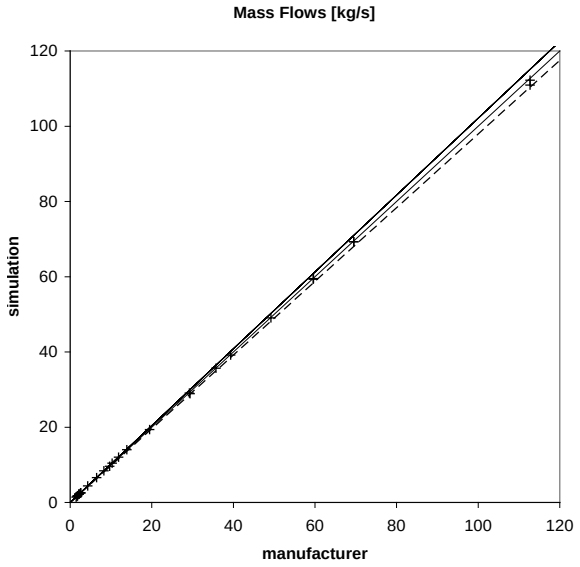

Fig. 20. Simulated mass flows vs. manufacturer's data (design case).

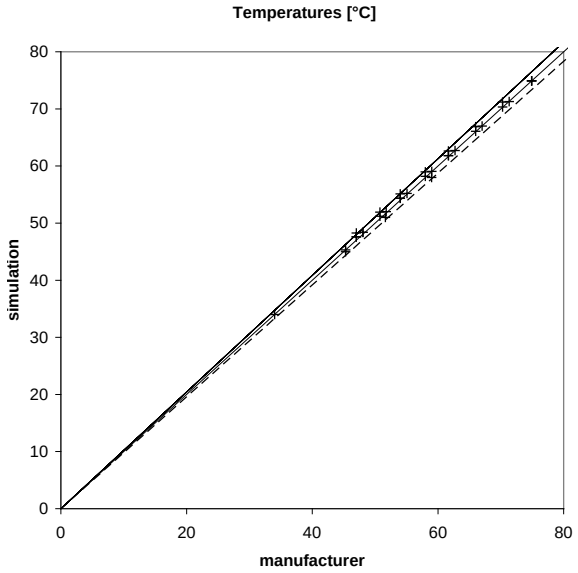

Fig. 21. Simulated temperatures vs. manufacturer's data (design case).

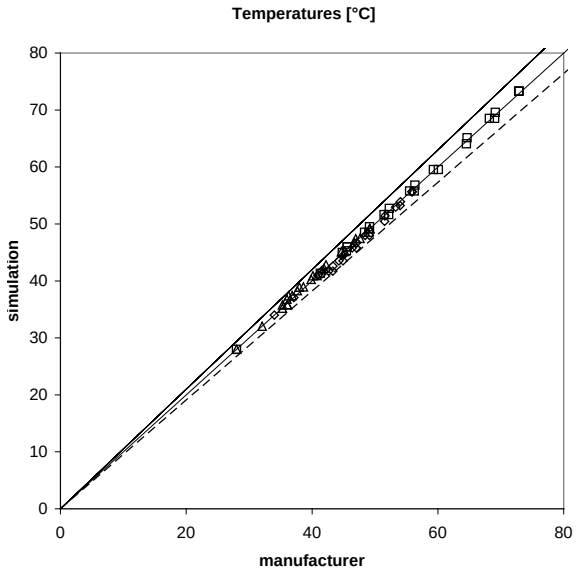

Fig. 23. Simulated temperatures vs. manufacturer's data (off-design case).

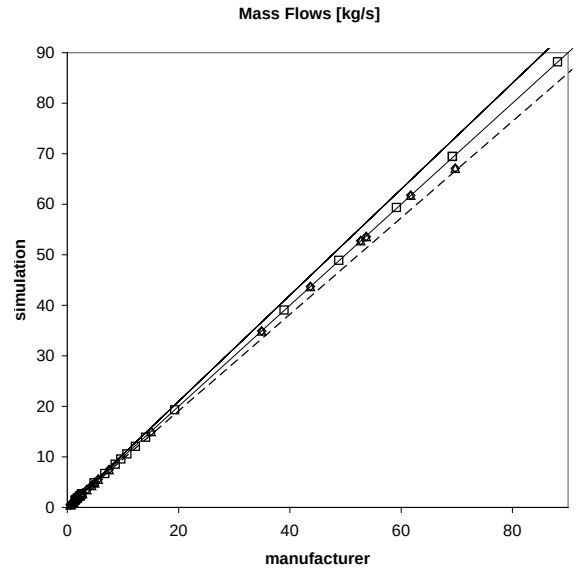

Fig. 22. Simulated mass flows vs. manufacturer's data (off-design case).

6. Outlook and conclusion

A more accurate description of the equation of state for seawater has currently been released by the International Association for the Properties of Water and Steam [21]. The properties described therein are related to the IAPSO Standard Seawater [22] and present a fundamental equation for the Gibbs energy as a function of salinity, temperature and pressure relative to the Gibbs energy of pure water. The equation is consistent with the IAPWS-95 formulation for the fluid phase of water and is valid within a temperature range of –2 to 80°C and a salinity of up to 120 g/kg.

Vapour from flashing brine is supposed to pass the tube bundle without condensation. In reality partial condensation takes place. This is to be considered when advancing the current MED model.

The comparison of different correlations clearly brought out significant deviations in heat transfer prediction. Utmost attention has to be paid to the proper selection of the relevant approach. Further investigations in this regard are highly recommended, extending the current work to further heat transfer correlations available. In the course of these further investigations influences on the heat transfer like superheated or wet steam fed to the tube bundle might be considered as well as possible subcooling of condensate.

Not taken into account so far were pressure losses of any kind. The most effecting losses occur during the condensation inside the tubes as well as during evaporation within the tube bundle. Bend losses especially in case of multiple pass tube bundles are to be considered as well.

The current thermal vapour compressor model is suitable for design calculations only. An enhanced model has to be developed to enable appropriate calculation of off-design cases as well.

7. Symbols

A — Area, m²
C — Constant
c_p — Specific heat capacity, kJ/kgK
D — Diameter, m
d_h — Hydraulic diameter, m

F — Flow parameter
FF — Fouling factor, m²K/kW
Fr — Froude number
g — Gravity, m/s²
Ga — Galileo number
h — Enthalpy, kJ/kg
Ja — Jakob number
K — Constant
K_{Ph} — Correction factor
K_W — Correction factor for vertical walls
Ka — Kapitza number
L — (Characteristic) length, m
$\dot{m}$ — Mass flow, kg/s
M — Molar mass, g/mol
N_{tubes} — Number of tubes
Nu — Nusselt number
p — Pressure, bar
Pr — Prandtl number
Q — Transferred heat, kW
Re — Reynolds number
r — Ratio
s — Tube pitch, m
s — Entropy, kJ/kgK
T, t — Temperature, °C
u — Velocity, m/s
$U_{overall}$ — Overall heat transfer coefficient, kW/m²K
w — Mass fraction (total dissolved solids), kg/kg
x — Steam quality (kg vapour/kg liquid), kg/kg
X_{tt} — Martinelli parameter

Greek

α — Heat transfer coefficient, kW/m²K
β — Factor
Γ — Spray density, kg/ms
δ_A^+ — Thickness of liquid cross sectional area averaged over the perimeter, m
ε —- Volumetric vapour content
η —- Dynamic viscosity, Pas
λ —- Thermal conductivity, W/mK
ν —- Kinematic viscosity, m²/s
ξ —- Resistance coefficient
ρ —- Density, kg/m³
σ —- Surface tension, kg/s²
τ —- Shear stress, kg/ms²
τ^* —- Shear stress dimensionless
φ —- Circumferential angle, rad
Φ —- Angle of draining condensate, rad

Indices

0 — Initial
brine_br — Part of brine not flashing off
brine_rw — Part of raw water not flashing off
cond_hot — Condensate from effect
drain_br — Brine from effect
drain_cond — Part of condensate not flashing off
drain_cold — Seawater drain
drain_hot — Condensate from heating steam
drain_steam — Vapour from effect
evap — Evaporation
feed_1 — Suction steam
feed_2 — Motive steam
feed_br — Brine feed
feed_cond — Condensate feed
feed_cold — Seawater feed
feed_hot — Heating steam feed
feed_rw — Raw water feed
flash_rw — Vapour from flashed off raw water
i — Inner
in — Incoming
l — Liquid
lam — Laminar
liquid_rw — Part of feed raw water not flashing off
m — Mean value
NC-Gases — Non condensable gases
o — Outer
out — Outgoing
pre — Preheating
rw — Raw water
red — Reduced
S — Salt
sat — Saturation
steam_br — Vapour from flashed off brine
steam_cond — Vapour from flashed off condensate
steam_rw — Vapour from evaporated raw water
strat — Stratified
sw — Seawater
th — Thermal
th,dev — Thermal developing region
th,fully — Thermal fully developed region
turb — Turbulent
v — Vapour
W — Wall
x — Position x

References

[1] T. Altmann, A. Attenborough and M. Rieder, Modelling and Optimization of Dual Purpose Power and Desalination Plants. IDAWC/MP07-246.
[2] S. Bergmann and E. Perz, Modelling integrated power and desalination plants. Proc. Power-Gen Middle East Conference, 2004.
[3] H.U. Sverdrup, M.W. Johnson and H.R. Fleming, The Oceans, Their Physics, Chemistry, and General Biology. New York, Prentice-Hall, 1942.
[4] F.J. Millero, R. Feistel, D.G. Wright and T.J. McDougall, The Composition of Standard Seawater and the Definition of the Reference-Composition Salinity Scale, Deep-Sea Research I 55 (2008) 50–72, Elsevier, 2007.
[5] B. Arzt, Meerwasserentsalzung durch Mehrfacheffekt-Stack-Horizontalrohrverdampfung. Dissertation. Technical University Aachen, 1984.
[6] International Association for Properties of Water and Steam. The Thermodynamic Properties of Water and Steam, 1997, http://www.iapws.org.

[7] A. Husain, K. Wangnick and A. Radif, Case study on planning a large scale multistage flash desalination plant. Encyclopaedia of Desalination and Water Resources, EOLSS Publishers, Oxford, http://www.desware.net.
[8] H.E. Hoemig, Seawater and Seawater Distillation. Vulkan-Verlag, 1978.
[9] J. Thome, Engineering Data Handbook III. Wolverine Tube, Inc., 2004.
[10] VDI-Gesellschaft Verfahrenstechnik und Chemieingenieurwesen. VDI-Waermeatlas, 10, Auflage, Springer Verlag, 2006.
[11] L.D. Boyko and G.N. Kruzhilin, Heat transfer and hydraulic resistance during condensation of steam in a horizontal tube and in a bundle of tubes. Intern. J. Heat Mass Transfer, 10 (1967) 361-373.
[12] H. Jaster and P.G. Kosky, Condensation heat transfer in a mixed flow regime. Intern. J. Heat Mass Transfer, 19 (1976) 95-99.
[13] J. Widua, Zum Einsatz der Seeding Technik im Horizontalrohrverdampfer bei der Eindampfung haertebildender, waessriger Loesungen, VDI-Fortschrittsberichte, Reihe 3, Nr. 410, VDI-Verlag, 1995.
[14] W.L. Owens, Correlation of thin film evaporation heat transfer coefficients for horizontal tubes. Proc. 5th Ocean Thermal Energy Conversion Conference, 6 (1978) 71–89.
[15] K.R. Chun and R.A. Seban, Heat transfer to evaporating liquid films. J. Heat Transfer, 93 (1971) 391-396.
[16] J.C. Han and L.S. Fletcher, Falling film evaporation and boiling in circumferential and Axial grooves on horizontal tubes. Indust. Eng. Chem. Process Design Devel., 24 (1985) 570–575.
[17] Y. Fujita and M. Tsutsui, Experimental investigation of falling film evaporation on horizontal tubes. Heat Transfer – Japan. Res., 27(8) (1998) 609-618.
[18] J.J. Lorenz and D. Yung, A note on combined boiling and evaporation of liquid films on horizontal tubes. J. Heat Transfer, ASME, 101 (1979) 178-180.
[19] J.M. Coulson and J.F. Richardson, Coulson and Richardson's Chemical Engineering, Vol. 1, 6th ed., Butterworth-Heinemann, 1999.
[20] H.D. Baehr, Thermodynamik. 6 Auflage, Springer Verlag, 1988.
[21] International Association for Properties of Water and Steam, The Thermodynamic Properties of Seawater, 2008, http://www.iapws.org.
[22] F. Culkin and P. S. Ridout, Stability of IAPSO Standard Seawater. J. Atm. Ocean Technol., 15 (1998)1072.